Journal of Molecular Spectroscopy 283 (2013) 32–43

Contents lists available at SciVerse ScienceDirect

Journal of Molecular Spectroscopy

journal homepage: www.elsevier.com/locate/jms

Direct-potential-fit analysis for the $A^3\Pi_{1u}$–$X^1\Sigma_g^+$ system of Br_2

Tokio Yukiya [a,*], Nobuo Nishimiya [b], Yoko Samejima [b], Koji Yamaguchi [b], Masao Suzuki [b], Christopher D. Boone [c], Irving Ozier [d], Robert J. Le Roy [c]

[a] Department of Applied Computer Science, Tokyo Polytechnic University, 1583 Iiyama, Atsugi, Kanagawa 243-0297, Japan
[b] Department of System Electronics and Information Technology, Tokyo Polytechnic University, 1583 Iiyama, Atsugi, Kanagawa 243-0297, Japan
[c] Department of Chemistry, University of Waterloo, Waterloo, Ontario, Canada N2L 3G1
[d] Department of Physics and Astronomy, University of British Columbia, 6224 Agricultural Road, Vancouver, British Columbia, Canada V6T 1Z1

ARTICLE INFO

Article history:
Received 13 October 2012
In revised form 14 December 2012
Available online 4 January 2013

Keywords:
Diatomic halogen
Br_2
Potential energy function
Titanium sapphire laser
Electronic isotope shift

ABSTRACT

Doppler-limited rovibrational absorption spectra of the $A^3\Pi_{1u} \leftarrow X^1\Sigma_g^+$ electronic transition of Br_2 are measured in the 12072–14249 cm^{-1} region by a tone burst modulation method using a Ti:sapphire ring laser. *P*-, *Q*-, and *R*-branch lines belonging to the $v' \leftarrow v'' = (2\text{–}16) \leftarrow (2\text{–}8)$ bands of $^{79,79}Br_2$ and $^{79,81}Br_2$, and the $v' \leftarrow v'' = (2\text{–}5) \leftarrow 6$ bands of $^{81,81}Br_2$ are observed and assigned. Accurate analytic potential energy functions for the $A^3\Pi_{1u}$ and $X^1\Sigma_g^+$ states are determined from a combined-isotopologue direct-potential-fit analysis of these data together with all other available high quality data for the *A* and *X* states. This work also yields a slightly improved ground-state well depth $\mathfrak{D}_e(X) = 16056.875(2)\ cm^{-1}$ and dissociation energy $\mathfrak{D}_0(X) = 15894.495(2)\ cm^{-1}$ for $^{79,79}Br_2$, and shows that the isotope shift of the *A*–*X* electronic transition energy $T_e^{81,81} - T_e^{79,79} = -0.016(3)\ cm^{-1}$ is likely mainly due to the isotopologue dependence of the*X*-state well depth.

1. Introduction

The $A^3\Pi_{1u}$–$X^1\Sigma_g^+$ system of Br_2 has been studied by many researchers. It was first observed in 1926 by Kuhn [1] and Nakamura [2] who published vibrational analyses of its absorption spectrum in the 5117–6722 and 5130–7586 Å regions, respectively. In 1931 Brown extended their results by using a grating spectrometer to study Br_2 absorption in the 5100–7600 Å region, and reported vibrational assignments for band heads that he tentatively identified as being associated with $v' = 0\text{–}21$ and $v'' = 1\text{–}5$ [3]. Five years later Darbyshire used a prism instrument to study high temperature samples in the 7600–8180 Å region [4]. This allowed him to extend the ground-state vibrational range to $v'' = 13$ and to observe two *A*-state vibrational levels lying below the lowest one that Brown had seen.

The first rotational analysis for the $A^3\Pi_{1u}$–$X^1\Sigma_g^+$ system was reported by Horsley in 1967 [5]. He measured the absorption spectrum of natural bromine in the 6400–7100 Å region, and assigned the *Q*-branch lines of bands identified as $v' \leftarrow v'' = (13\text{–}19) \leftarrow 2$ and $(16,17) \leftarrow 3$ of $^{79,81}Br_2$. However, the absolute vibrational numbering for the *A* state remained unclear. In that same year Clyne and Coxon measured the band structure of Br_2 in the 6400–10000 Å region in emission, but again the absolute vibrational numbering in the *A* state remained unsettled [6]. Finally, in 1970 Coxon and Clyne measured the absorption spectrum of a few bands of isotopically pure $^{79,79}Br_2$ with rotational resolution [7], and by comparing their results with the $^{79,81}Br_2$ measurements of Horsley [5], they confirmed Darbyshire's hypothesis [4] that the tentative *A*-state vibrational labels proposed by Brown [3] should be increased by seven. Shortly after this, Coxon extended his rotational resolution studies of the $A^3\Pi_{1u}$–$X^1\Sigma_g^+$ system to span almost 50% of the *A*-state well ($v' = 7\text{–}24$) [8], and reported extended sets of Franck–Condon factors and R-centroids for this system [9]. These studies provided a good basic understanding of the $A^3\Pi_{1u}$ state of Br_2, and facilitated its use in studying a number of ion-pair states [10–15]. Moreover, one of these studies of ion-pair states reported a handful of observations of *A*-state levels $v = 30\text{–}35$ [10], and another reported observations of $v(A) = 0$ [15]. However, all of this early work has since been superseded by measurements of higher precision spanning an even wider range of levels. An overview of the data, on which the present analysis is based, is presented in Table 1. The average relative discrepancies shown in its second-last column are based on the final recommended potential energy function model of Section 4. The fact that all values of this average relative discrepancy are $\ll 1$ shows that there are no significant calibration error inconsistencies among the various data subsets.

In 1999 Boone used Doppler-limited magnetic rotation spectroscopy with a dye laser [16,17] to measure and assign some 3263 lines of 51 bands in the $A^3\Pi_{1u} \leftarrow X^1\Sigma_g^+$ spectrum of $^{79,79}Br_2$, involving *A*-state vibrational levels $v' = 13\text{–}37$. The highest

* Corresponding author.
E-mail address: yukiya@cs.t-kougei.ac.jp (T. Yukiya).

0022-2852/$ - see front matter © 2013 Elsevier Inc. All rights reserved.
http://dx.doi.org/10.1016/j.jms.2012.12.006

Table 1
Summary of data used in the present analysis; uncertainties are in cm^{-1}.

Type	No. data	Uncertainty	Range $v'(A)$	Range $v''(X)$	Average $\{\frac{calc.-obs.}{unc}\}$	Source
$^{79,79}Br_2$						
B–X absorption[a]	1515	0.0020	N/A	0–14	0.0014	Gerstenkorn et al. [18]
B–X fluorescence	257	0.01	N/A	3–29	0.0021	Focsa et al. [19]
B–X fluorescence	8	0.27	N/A	29–35	−0.0010	Postell [20]
A–X magnetic rotation	2992	0.0035	13–37[b]	0–2	−0.0048	Boone [16]
A–X laser absorption	4246	0.0030	2–16	2–8	−0.0139	Present
$^{81,81}Br_2$						
A–X laser absorption	338	0.0030	2–5	6	−0.1506	Present
B–X fluorescence	345	0.01	N/A	3–29	0.0088	Focsa et al. [19]
B–X fluorescence	9	0.27	N/A	28–43	−0.0096	Postell [20]
$^{79,81}Br_2$						
A–X absorption	5350	0.0030	2–16	2–8	0.0127	Present
B–X fluorescence	1182	0.01	N/A	2–29	0.0055	Focsa et al.
B–X fluorescence	94	0.27	N/A	28–44	−0.0017	Postell [20]
VUV fluorescence	578	0.06	N/A	0–76	−0.0232	Venkateswarlu et al. [22]

[a] Synthetic data consisting of term values for v'' = 0–14, J'' = 0–100 generated from the constants of Gerstenkorn et al. [18], as described by Focsa et al. [19], treated as a fluorescence series in the analysis.
[b] Transitions involving $v(A)$ = 27 were not used in the analysis.

vibrational level he observed is bound by only 2 cm^{-1}. This is less than half the binding energy of the highest observed level of the $B^3\Pi_{0_u^+}$ state [18], and hence should allow an improved determination of the Br_2 dissociation energy. Boone performed both a conventional Dunham expansion analysis and a 'Near-Dissociation-Expansion' analysis, and those results can be found in his thesis [16]. However, the lowest observed level of the A state was still $v(A)$ = 7 [8], which lies almost 1000 cm^{-1} above the A-state potential minimum.

In the present work, rovibrational absorption spectra of the $A \leftarrow X$ transition of Br_2 were measured in the 12 072–14 249 cm^{-1} region, and P-, Q-, and R-branch progressions of 109 bands in this system were assigned. The observed vibrational levels of $^{79,79}Br_2$ and $^{79,81}Br_2$ in the A and X state are v' = 2–16 and v'' = 2–8, respectively, and those of $^{81,81}Br_2$ are v' = 2–5 and v'' = 6, while the associated rotational sublevels range up to J = 99. Thus, the high-resolution data (uncertainties <0.01 cm^{-1}) for the A state used in the present analysis extend from $v(A)$ = 2–37, with the highest observed vibrational level lying less than 2 cm^{-1} below the dissociation limit. A schematic overview of this system is presented in Fig. 1.

Unfortunately, the high-resolution A–X data described above only span a small portion of the $X^1\Sigma_g^+$ state potential well (v'' = 0–8). Since we wish also to obtain the best possible overall description of the $X^1\Sigma_g^+$ ground state, the present analysis also incorporated the laser-induced fluorescence Fourier Transform (FT) results of Focsa et al. [19] for the B–X system, which extend from $v(X)$ = 2–29 for $^{79,81}Br_2$ and from $v(X)$ = 3–29 for $^{79,79}Br_2$ and $^{81,81}Br_2$. Following Focsa et al., our analysis also incorporates the 1515 synthetic term values for levels v'' = 0–14 of the ground state of $^{79,79}Br_2$ that they had generated from the molecular constants of Gerstenkorn et al. [18], and treated as a synthetic fluorescence series. However, even with this inclusion, the data range only span 54% of the ground-state potential well.

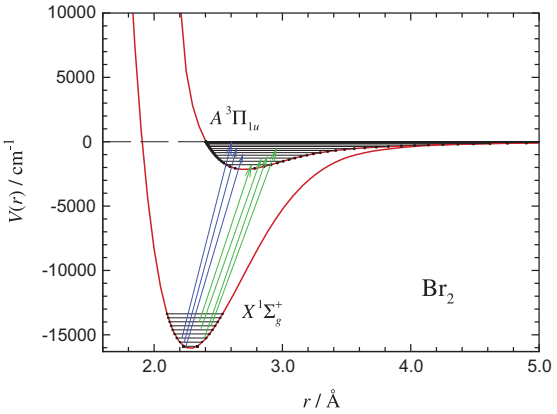

Fig. 1. Overview of the $A^3\Pi_{1u}$–$X^1\Sigma_g^+$ system of Br_2 with representative magnetic rotation transitions [16] shown in blue and laser absorption transitions (present work) in green. (For interpretation of the references to colour in this figure legend, the reader is referred to the web version of this article.)

More recently, Postell et al. performed laser-induced fluorescence measurements that extended this range to $v(X)$ = 44, which is 75% of the way to dissociation [20,21]. Although their data have relatively low precision (±0.27 cm^{-1}), since they include results for all three isotopologues and extend the range to cover 3/4 of the potential well, they are also used in our analysis (weighted appropriately). The final set of X-state data included in the present analysis were then the 12 VUV resonance fluorescence series reported in 1982 by Venkteswarlu et al. [22]. Although these data span the range v'' = 0–76, they were pointedly omitted from the analysis of Focsa et al. because the 1982 molecular constants seemed inconsistent with their new higher accuracy (±0.01 *vs.* ±0.06 cm^{-1}) FT results for v'' = 2–29 [19]. However, although the constants may be inconsistent, we find that within the reported uncertainties, the actual VUV data are entirely compatible with the higher resolution data. Hence, these VUV fluorescence series data were also utilized in the present analysis. As a result, our data for the $X^1\Sigma_g^+$ state span 99.2% of the ground-state potential well, with the highest observed level (v = 76) being bound by 129 cm^{-1}. However, since the $A^3\Pi_{1u}$ and $X^1\Sigma_g^+$ states have the same asymptote, the present analysis should yield an improved estimate of the ground-state dissociation energy.

In the following, Section 2 describes our new laser absorption measurements for the three isotopologues of Br_2. Section 3 then describes our method of analysis and the models used for the potential energy and Born–Oppenheimer breakdown functions, while Section 4 presents our results.

2. Experimental

2.1. Methodology

Fig. 2 presents a schematic view of the experimental setup. A titanium sapphire ring laser (Coherent, 899-21) pumped by an

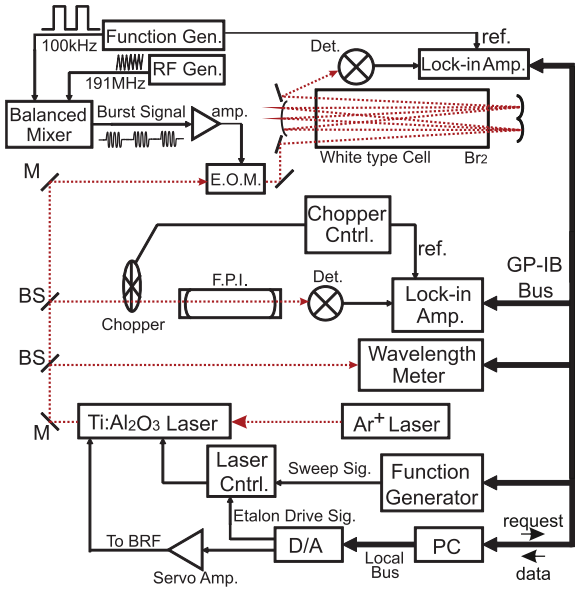

Fig. 2. Block diagram of the Ti:Sapphire ring laser spectrometer.

argon ion laser (Coherent, Innova 300) was used to obtain our Doppler limited absorption spectra. The absorption occurred in a White-type cell with an effective path length of 13.6 m that was filled with Br_2 gas at 10 Torr, with the three isotopologues present in natural abundance. Measurements at wavelengths shorter than 0.77 μm, were made with the cell at room temperature, while for those at longer wavelengths the cell was heated to 150 °C.

Tone burst modulation was adopted as the signal detection technique [23]. The laser source sidebands were produced using an electro-optical modulator (EOM). A burst signal was generated by a balanced mixer using this 191 MHz source and square-wave modulation at 100 kHz. Relative frequencies were measured by generating fringe markers using a confocal cavity (F.P.I. in Fig. 2) with a free spectral range of 0.01 cm^{-1}. Absolute wavelengths were determined using a wavelength metre (Burleigh WA-1500) that was calibrated using the two-photon signal of ^{85}Rb at 778 nm, and has an estimated uncertainty of 0.03 cm^{-1}.

The continuous tuning range of this laser system is only 20 GHz, with the tuning being driven by a sweep signal produced using a function generator (see Fig. 2). To scan a broad wavelength region, the birefringent-filter and etalon in the ring cavity were adjusted after every 20 GHz sweep using a D/A converter attached to a PC. In addition, by means of a GP-IB bus, the PC controlled the lock-in amplifiers, the wavelength metre, and the function generator producing the sweep signal. The PC also stored the resulting data measurements. Line positions in the absorption spectrum were determined using the wavemeter in the manner reported by Yukiya et al. [24]. The intensities of the laser beams seen via the White-type cell or the F.P.I. were measured by PIN photo-diode detectors.

In order to characterize our measurement accuracy and check for mis-assigned lines, we performed a preliminary analysis in which the line positions were fitted to an expression that used band constants for the A state, and Dunham expansions for the X state:

$$\nu(v',J';v'',J'') = T_{v'} + B^{e/f}_{v'}\{J'(J'+1) - \Omega^2\} - D_{v'}\{J'(J'+1) - \Omega^2\}^2 + H_{v'}\{J'(J'+1) - \Omega^2\}^3 + \cdots - \sum_{l=1}\sum_{m=0} Y''^{\alpha}_{l,m}(v''+1/2)^l\{J''(J''+1)\}^m. \quad (1)$$

Here, the X-state $Y''^{\alpha}_{l,m}$ values for different isotopologues (α_1, α_2) were related by conventional first-order semiclassical scaling by powers of the ratio of reduced masses, $Y^{\alpha_1}_{l,m}/Y^{\alpha_2}_{l,m} = (\mu_{\alpha_2}/\mu_{\alpha_1})^{m+l/2}$. In the A state, the e and f parity sublevels are separated by the Ω-doubling interaction characterized by the molecular constants $q_{v'}$. In the A–X system, the f and e levels, respectively, are the upper levels of the Q- and of the P- and R-transitions. To take the Ω-doubling into account, independent values of the inertial rotational constant, $B^f_{v'}$ and $B^e_{v'} = B^f_{v'} + q_{v'}$, respectively, are used [25]. An empirical fit to Eq. (1) that was 'saturated' with respect to the number of parameters being used has a root mean square deviation of 0.003 cm^{-1}, and a histogram of those deviations shows the expected Gaussian shape. Hence 0.0030 cm^{-1} is the uncertainty used to weight the present data in our fits.

2.2. Results

In contrast with some of the previous work on this system [16,18], the present experiments did not use isotopically purified Br_2 gas, so our absorption spectrum consists of overlapping series of P-, Q- and R-branch lines from all three species: $^{79}Br_2$, $^{79,81}Br_2$ and $^{81}Br_2$. Fig. 3 shows a recorder trace of the Doppler-limited absorption spectrum detected by our tone-burst technique for the interval 12 711.0–12 713.5 cm^{-1}. The approximately equal natural abundances of ^{79}Br and ^{81}Br give rise to intensity ratios of 1:2:1 for lines of $^{79,79}Br_2$, $^{79,81}Br_2$ and $^{81,81}Br_2$, respectively. Our analysis readily discerns the Ω-doubling splitting in the A state. However, because the nuclear quadrupole coupling constants for both bromine isotopes are only half of that for iodine, our Doppler-limited spectrum could not resolve the nuclear-quadrupole-induced splitting of the P-, and R-branch lines, although it was readily observed in the $A \leftarrow X$ systems of ICl, I_2 and IBr [24,26–28].

The present study observed transitions involving vibrational levels $v' = 2$–16 of the A state and $v'' = 2$–8 of the X state for $^{79,79}Br_2$ and $^{79,81}Br_2$, as well as $v' \leftarrow v'' = (2–5) \leftarrow 6$ transitions of $^{81}Br_2$. These 9334 assigned lines in 108 bands include the first ever observation of levels $v'(A) = 2$–6. As was outlined in Section 1, in order to obtain the most comprehensive description possible for the A and X states, the present analysis combines our new results

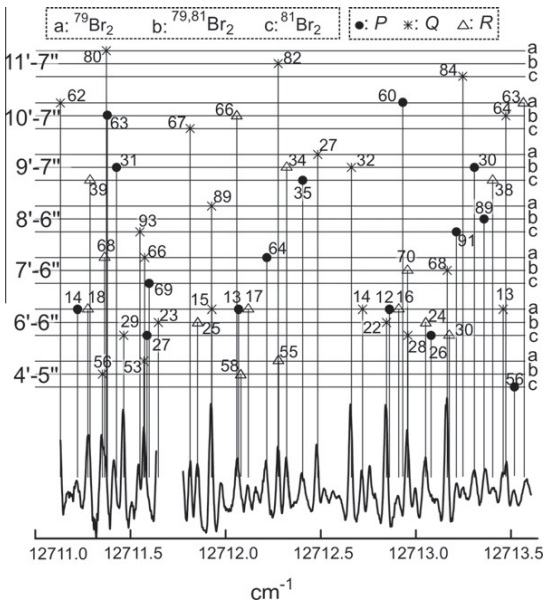

Fig. 3. Recorder trace of Br_2 absorption lines in the 12 711.0–12 713.5 cm^{-1} region.

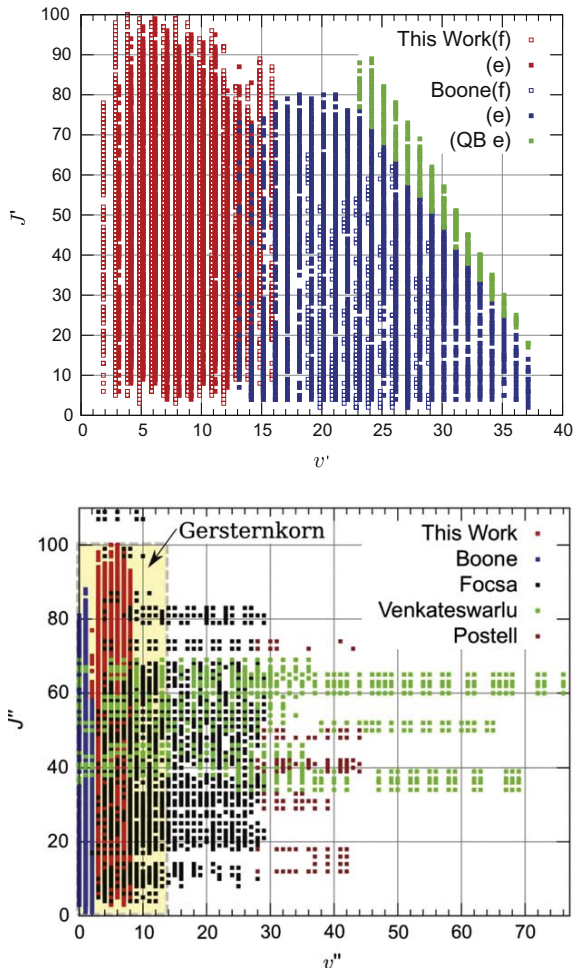

Fig. 4. Assigned vib-rotational levels of the Upper: $A^3\Pi_{1u}$ state, with open points for *f*-levels, solid points for *e*-levels, 'QB' for quasibound levels, and Lower: $X^1\Sigma_g^+$ state of Br_2.

with the earlier data of Venkateswarlu et al. [22], Gerstenkorn et al. [18], Boone [16], Focsa et al. [19], and Postell [20,21]. Overviews of these data are presented in Fig. 4 and Table 1. These data span 99.2% of the *X*-state potential energy well, and extend from $v = 2$ up to $v = 37$ for the *A* state, which is 99.91% of the way to dissociation. Note, however, that following Boone [16], his 269 data involving *A*-state level $v' = 27$ were omitted from our analysis because they displayed irregular behaviour and could not be systematically accounted for by any of the models considered. A complete listing of the experimental data used in the present work is included in the Supplementary data submitted to the Journal.

3. Analysis

3.1. Methodology

The main part of the present analysis was performed using a direct-potential-fit (DPF) method in which simulated spectra generated using a radial Hamiltonian $\widehat{\mathcal{H}} = \widehat{\mathcal{H}}(\{p_j\})$ defined in terms of parameterized potential energy, Born–Oppenheimer breakdown (BOB), and Ω-doubling strength functions, are compared with experiment, and the parameters $\{p_j\}$ are optimized by a standard non-linear least-squares-fit technique [29]. The partial derivatives of the eigenvalues with respect to the parameters of the Hamiltonian that were required by the least-squares procedure were generated from the Hellman–Feynman theorem expression

$$\frac{\partial E_{vJ}}{\partial p_j} = \left\langle \psi_{vJ} \left| \frac{\partial \widehat{\mathcal{H}}}{\partial p_j} \right| \psi_{vJ} \right\rangle, \tag{2}$$

where the eigenfunctions $\psi_{vJ}(r)$ are obtained when solving the radial Schrödinger equation for the level energies in order to simulate the spectra. The quality of a fit is characterized by the dimensionless root-mean-square deviations between the *N* simulated data $y_i^{\rm calc}$ and the corresponding experimental values $y_i^{\rm obs}$:

$$\overline{dd} \equiv \left\{ \frac{1}{N} \sum_{i=1}^{N} \left(\frac{y_i^{\rm calc} - y_i^{\rm obs}}{u_i} \right)^2 \right\}^{1/2} \tag{3}$$

in which u_i is the uncertainty associated with datum-*i*. While most of these uncertainties are set at the characteristic value associated with a given data set (see Table 1), those associated with the highest-*J* lines for a given branch are sometimes somewhat larger, and those for transitions in which the upper or lower level is 'quasibound', lying above the dissociation limit but below the top of a potential energy barrier, are defined as

$$u_i^{\rm eff} = \sqrt{\left(u_i^{\rm exp}\right)^2 + (0.2\Gamma_i)^2} \tag{4}$$

in which Γ_i is the tunnelling predissociation width of quasibound level $E_{vJ}(i)$, which is calculated as described in Ref. [30], and the factor of 0.2 is based on the experience of Refs. [31,32].

3.2. The radial Hamiltonian

As in most DPF analyses reported to date, the present work uses a form of the effective radial Hamiltonian introduced by Watson in which BOB terms associated with the radial kinetic energy operator are incorporated into both an effective 'adiabatic' correction to the rotationless potential, and the non-adiabatic centrifugal BOB correction [33,34]. Following the convention of Ref. [35] for the mass-scaling of the BOB terms, and that of Ref. [30] for describing Ω-doubling, the effective radial Hamiltonian used in the present work is defined by

$$\begin{aligned}\widehat{\mathcal{H}}\psi_{vJ}(r) = \Bigg\{ & -\frac{\hbar^2}{2\mu_\alpha}\frac{d^2}{dr^2}\left[V_{\rm ad}^{(1)}(r) + \Delta V_{\rm ad}^{(\alpha)}(r)\right] \\ & + \frac{[J(J+1)-\Omega^2]}{2\mu_\alpha r^2}[1 + g^{(\alpha)}(r)] + sg_\Omega(e/f)\Delta V_\Omega^{(\alpha)}(r)[J(J+1)]^A \Bigg\}\psi_{vJ}(r) \\ & = E_{vJ}\psi_{vJ}(r).\end{aligned}$$

Here, $V_{\rm ad}^{(1)}(r)$ is the effective adiabatic potential for the selected reference isotopologue (labelled $\alpha = 1$), and $\Delta V_{\rm ad}^{(\alpha)}(r)$ is the difference between the effective adiabatic potentials for isotopologue-α and that for the reference species ($\alpha = 1$), while $g^{(\alpha)}(r)$ is the non-adiabatic correction to the effective centrifugal potential term. In addition, $sg_\Omega(e/f)$ is a dimensionless numerical factor which is zero when there is no Ω-doubling (i.e. for the $X^1\Sigma_g^+$ state of Br_2), and has numerical values of zero or ±1 for the *e*- and *f*-levels of states with $\Omega \neq 0$ [29,30,36]. For the $A^3\Pi_{1u}$ state we select the *e*-parity levels as the reference states, and hence $sg_\Omega(e) = 0$ and $sg_\Omega(f) = -1$. The potential energy and centrifugal BOB functions are each written as a sum of terms, one for each of atoms *A* and *B*:

$$\Delta V_{\rm ad}^{(\alpha)}(r) = \frac{\Delta M_A^{(\alpha)}}{M_A^{(\alpha)}}\widetilde{S}_{\rm ad}^A(r) + \frac{\Delta M_B^{(\alpha)}}{M_B^{(\alpha)}}\widetilde{S}_{\rm ad}^B(r); \tag{6}$$

$$g^{(\alpha)}(r) = \frac{M_A^{(1)}}{M_A^{(\alpha)}}\widetilde{R}_{\rm na}^A(r) + \frac{M_B^{(1)}}{M_B^{(\alpha)}}\widetilde{R}_{\rm na}^B(r). \tag{7}$$

Here, $\Delta M_A^{(\alpha)} = M_A^{(\alpha)} - M_A^{(1)}$ is the difference between the atomic mass of atom A in isotopologue-$\alpha\left(M_A^{(\alpha)}\right)$ and in the reference isotopologue $\left(M_A^{(1)}\right)$, and analogous definitions apply for atom B. The Ω-doubling (or Λ-doubling) radial strength function is then written as the product [29,30,36]:

$$\Delta V_\Omega^{(\alpha)}(r) = \left(\frac{\hbar^2}{2\mu_\alpha r^2}\right)^{2\Omega} f_\Omega(r). \tag{8}$$

3.3. Models for the potential energy, Born–Oppenheimer breakdown, and Ω-doubling functions

The X and A state potential energy functions $V_{\rm ad}^{(1)}(r)$ are represented by "Morse/Long-Range" (MLR) functions which have the form [37,38]:

$$V_{\rm MLR}(r) = \mathfrak{D}_e\left\{1 - \frac{u_{\rm LR}(r)}{u_{\rm LR}(r_e)} e^{-\beta(r)\cdot y_p(r;r_e)}\right\}^2. \tag{9}$$

Here, $\mathfrak{D}_e$ is the well depth, r_e is the equilibrium internuclear distance, $u_{\rm LR}(r)$ defines the attractive long-range tail of the potential, and $u_{\rm LR}(r_e)$ is the value of that function at $r = r_e$. In the exponent of Eq. (9),

$$y_p(r;r_e) \equiv \frac{r^p - r_e^p}{r^p + r_e^p} \tag{10}$$

is a dimensionless radial variable, with p being a small positive integer (see below). The exponent coefficient function $\beta(r)$ is defined so that

$$\lim_{r\to\infty}\beta(r) \equiv \beta_\infty = \ln\{2\mathfrak{D}_e/u_{\rm LR}(r_e)\} \tag{11}$$

and since $y_p(r;\, r_e) \to 1$ as $r \to \infty$, this means that at very large distances

$$V_{\rm MLR}(r) \simeq \mathfrak{D} - u_{\rm LR}(r) + \cdots, \tag{12}$$

where $\mathfrak{D}$ is the absolute energy at the dissociation limit. In order to impose the limiting behaviour of Eq. (11), the MLR exponent coefficient function is written as a constrained polynomial:

$$\beta(r) = \beta_{p,q}(r) = \beta_\infty y_p(r;r_{\rm ref}) + \left[1 - y_p(r;r_{\rm ref})\right]\sum_{i=0}^{N_\beta}\beta_i \cdot y_q(r;r_{\rm ref})^i \tag{13}$$

in which the two radial variables $y_p(r;\, r_{\rm ref})$ and $y_q(r;\, r_{\rm ref})$ have the same dimensionless form as $y_p(r;\, r_e)$ in Eq. (10), except that they are expressed relative to a different expansion centre, $r = r_{\rm ref}$, and they are defined in terms of separate (integer) powers, p and q:

$$y_p(r;r_{\rm ref}) \equiv \frac{r^p - r_{\rm ref}^p}{r^p + r_{\rm ref}^p}; \quad y_q(r;r_{\rm ref}) \equiv \frac{r^q - r_{\rm ref}^q}{r^q + r_{\rm ref}^q}. \tag{14}$$

As indicated by theory [39–44], the long-range potential tail can be written as a sum of damped inverse-power terms:

$$u_{\rm LR}(r) = \sum_{i=1}^{\rm last} D_{m_i}(r)\frac{C_{m_i}}{r^{m_i}}. \tag{15}$$

Since ground-state atomic Br is not in an S state, it has a permanent quadrupole moment. As a result, the leading term in the long-range potential for both the $X^1\Sigma_g^+$ and $A^3\Pi_{1u}$ states is the first-order quadrupole–quadrupole interaction energy corresponding to $m_1 = 5$ [39,42], and the next two are the leading second-order dispersion energy terms for which $m_2 = 6$ and $m_3 = 8$ [39–41,44]. Throughout most of this work C_5, C_6, and C_8 were fixed at the theoretical values of Saute et al. [45], although in some of the later fits the C_5 coefficient for the A state was treated as a free parameter. Damping functions $D_{m_i}(r)$ were introduced to take account of the weakening of the dispersion interaction at distances where the electron clouds on the interacting atoms overlap significantly [38,43,46]. The present work uses the modified Douketis-type [46] damping functions for $s = -1$ introduced in Ref. [38]:

$$D_{m_i}(r) = \left(1 - \exp\left\{-\frac{b\cdot(\rho r)}{m_i} - \frac{c\cdot(\rho r)^2}{\sqrt{m_i}}\right\}\right)^{m_i+s} \tag{16}$$

in which $b = 3.30$ and $c = 0.423$, and ρ is a system-dependent scaling parameter defined in terms of a ratio of atomic ionization energies [38,46] that has the value $\rho = 0.912$ for a pair of ground-state Br atoms. Damping function behaviour has not been studied for the first-order quadrupole–quadrupole interaction giving rise to the $m_1 = 5$ terms, but it is convenient to use Eq. (16) for that case too as it ensures physically sensible behaviour of the MLR potentials at very short distances [37,38].

As discussed in Refs. [47,38], the value of p in Eqs. (13) and (14) must be larger than the difference between the powers of the first and last terms in Eq. (15), $p > (m_{\rm last} - m_1)$, in order to prevent the long-range behaviour of the exponential term in Eq. (9) from changing the effective values of one or more of the C_{m_i} coefficients defining the $u_{LR}(r)$ function. However, there is no analogous constraint on the value of q, although experience suggests that the best choice is usually $3 \leqslant q \leqslant p$. Similarly, the value of $r_{\rm ref}$ has no physical significance, but setting it at an optimum distance (manually selected, see below) somewhere between r_e and the largest interatomic distance sampled by the data used in the analysis (the outer turning point of the highest observed vibrational level) allows us to obtain an optimum representation of the data with the smallest number of fitted β_i exponent coefficients.[1]

Physical arguments regarding the limiting asymptotic values of the BOB functions of Eqs. (6) and (7) [48] make it appropriate to write the associated radial strength functions in the same type of form used for Eq. (13):

$$\widetilde{S}_{\rm ad}^A(r) = \widetilde{S}_\infty^A y_{p_{\rm ad}}(r;r_e) + [1 - y_{p_{\rm ad}}(r;r_e)]\sum_{i=0}^{N_{\rm ad}^A} u_i^A y_{q_{\rm ad}}(r;r_e)^i, \tag{17}$$

$$\widetilde{R}_{\rm na}^A(r) = \widetilde{R}_\infty^A y_{p_{\rm na}}(r;r_e) + [1 - y_{p_{\rm na}}(r;r_e)]\sum_{i=0}^{N_{\rm na}^A} t_i^A y_{q_{\rm na}}(r;r_e)^i \tag{18}$$

in which all of the radial y-variables have the form of Eq. (10). Since we choose to set the zero of energy at the energy of separated ground-state atoms, and neither of the Br atoms is charged, the limiting asymptotic values of these functions are $\widetilde{S}_\infty^{\rm Br} = \widetilde{R}_\infty^{\rm Br} = 0$, and the isotope dependence of the well depths is defined by the value of $u_0^{\rm Br}$ [48,49]. Since our molecule is comprised of two atoms of the same chemical species ($A = B = $ Br), this leads to the result:

$$\delta\mathfrak{D}_e^{(\alpha)} \equiv \mathfrak{D}_e^{(\alpha)} - \mathfrak{D}_e^{(1)} = \left\{\frac{\Delta M_{\rm Br(1)}^{(\alpha)}}{M_{\rm Br(1)}^{(\alpha)}} + \frac{\Delta M_{\rm Br(2)}^{(\alpha)}}{M_{\rm Br(2)}^{(\alpha)}}\right\}\left(\widetilde{S}_\infty^{\rm Br} - u_0^{\rm Br}\right). \tag{19}$$

In order to ensure that the effective adiabatic potentials for different isotopologues all have the same limiting long-range behaviour, we would normally set $p_{\rm ad} = m_1$ (=5 for Br_2) [48]. For the X state, however, the C_5/r^5 term is orders of magnitude weaker than the C_6/r^6 term over virtually the whole potential well. We therefore use $p_{\rm ad} = 6$ for the X state, while fixing $p_{\rm ad} = 5$ for the $A^3\Pi_{1u}$ state. There is no physical basis for specifying particular values for $q_{\rm ad}$, $p_{\rm na}$, or $q_{\rm na}$ [48], but in practise it is convenient to set $q_{\rm ad} = p_{\rm ad}$ and $q_{\rm na} = p_{\rm na}$, and we fix the latter two at $q_{\rm na} = p_{\rm na} = 3$. We also adopt the Watson convention of fixing $t_0^{\rm Br} = 0$, since this parameter is expected to be indeterminable from transition energy data alone

[1] A good preliminary estimate for $r_{\rm ref}$ is often the geometric mean of the inner and outer turning points of the highest observed level: $r_{\rm ref} \approx 3.0$ Å for the $X^1\Sigma_g^+$ state and 4.7 Å for the $A^3\Pi_{1u}$ state.

[33,34]. Finally, since we know of no physical constraints on the limiting asymptotic value or behaviour of the Ω-doubling radial strength function, we write it as a simple polynomial in the dimensionless radial variable of Eq. (10):

$$f_\Omega(r) = \sum_{i=0}^{N_\Omega} w_i^\Omega y_{q_\Omega}(r;r_e)^i. \quad (20)$$

Our earlier experience [48] indicated that use of very small values of the integer q_Ω tends to yield Ω-doubling strength functions $\Delta V_\Omega^{(\alpha)}(r)$ with implausible oscillatory behaviour outside the data region, and so we fix $q_\Omega = 4$.

3.4. Procedures

A particular MLR model, is defined by the terms included in Eq. (15) for $u_{\rm LR}(r)$ and by the values chosen for p, q, $r_{\rm ref}$ and the exponent polynomial order N_β in Eq. (13), and may be identified by the label $\mathrm{MLR}^{r_{\rm ref}}_{p,q}(N_\beta)$. The optimum recommended model is then chosen in order to minimize $\overline{dd}$ and the number of fitting parameters, together with the requirement that the resulting potential behave "sensibly" outside the data region, at both large and small r. Because we are dealing with a non-linear least-squares problem, in order to commence a particular DPF analysis it is necessary to have realistic initial trial estimates of the MLR parameters $\mathfrak{D}_e$, r_e, and the exponent polynomial expansion coefficients $\{\beta_i\}$ for each model considered. Fortunately, they are readily obtained by performing a preliminary empirical analysis using Dunham polynomial expressions for the level energies [50], generating RKR turning points from the resulting expressions [51,52], and then fitting the resulting turning points to Eq. (9). This last step was performed using computer program BETAFIT, which is available (with a manual) on the www [53]. In later stages of an analysis, such fits can be performed on potential function points generated from some earlier DPF run. Since the BOB functions and the Ω-doubling function are relatively weak, setting the initial trial values for all of the $\{u_i\}$, $\{t_i\}$ and $\{w_i\}$ coefficients equal to zero virtually always yields stable, convergent fits.

In the initial stage of a DPF analysis involving two (or more) electronic states, it is usually initially desirable to consider each state separately, so that correlations between the effects of parameters for the different states do not confuse the selection of the optimum model for each. This can be done readily with program DPOTFIT by requiring that the energy levels of all states other than the one of interest be represented by independent term values or band constants. In some cases this approach means that the fits involve a relatively large number of free parameters (more than 5600 when the $A^3\Pi_{1u}$ state of Br_2 is represented by term values), and hence they can be somewhat time consuming (requiring $\approx$1 CPU hour per cycle of fit in the above example), but they are otherwise robust and stable.

When one of the X or A states of Br_2 was represented by term values and the other by analytic potential energy, BOB and Ω-doubling functions, the quality of fit was not affected significantly by the inclusion of adiabatic potential-energy BOB functions $\Delta V_{\rm ad}^{(\alpha)}(r)$. However, when potential functions were used for both states, the quality of fit improved significantly (by 20%!) on allowing the first adiabatic BOB parameter, u_0, to be free for one or both states, although there was no significant further improvement when higher-order u_i were also allowed to vary. As is shown by Eq. (19), the value of u_0 determines the isotopologue-dependence of the well depth for a given state. The isotopologue-dependence of the electronic transition energy is therefore given by (since $\widetilde{S}_\infty^{\rm Br}(A) = \widetilde{S}_\infty^{\rm Br}(X) = 0$):

$$\delta T_e^{(\alpha)}(A-X) \equiv \delta\mathfrak{D}_e^{(\alpha)}(X) - \delta\mathfrak{D}_e^{(\alpha)}(A), \quad (21)$$

$$= \left\{ \frac{\Delta M^{(\alpha)}_{\mathrm{Br}(1)}}{M^{(\alpha)}_{\mathrm{Br}(1)}} + \frac{\Delta M^{(\alpha)}_{\mathrm{Br}(2)}}{M^{(\alpha)}_{\mathrm{Br}(2)}} \right\} \left(u_0^{\rm Br}(A) - u_0^{\rm Br}(X)\right). \quad (22)$$

Comparison of results for cases in which one or the other or both of $u_0^{\rm Br}(A)$ and $u_0^{\rm Br}(X)$ were allowed to vary freely showed that while the fitted values of these parameters varied significantly from case to case (sometimes even changing sign), the value of the difference $u_0^{\rm Br}(A)-u_0^{\rm Br}(X)$ was model-independent (within the uncertainties). We therefore conclude that the present analysis is able to determine the electronic isotope shift $\delta T_e^{(\alpha)}(A-X)$, but that the isotope-dependence of the individual well depths is less well defined. This conclusion was found to hold independent of what models were used for the potentials, for the non-adiabatic (centrifugal) BOB functions, or for the Ω-doubling radial strength functions, and our final recommended value for $\delta T_e^{(\alpha)}(A-X)$ is presented in Section 4.

When the energy levels of the A state were treated as independent term values, the quality of fit showed no significant improvement when one or more of the non-adiabatic centrifugal BOB parameters t_i for the X state was allowed to vary, and the resulting values of t_i always had uncertainties greater than 100%. We therefore conclude that the available data for the X state of Br_2 are not able to discern a non-adiabatic centrifugal BOB correction function. For the $A^3\Pi_{1u}$ state, however, the situation is quite different, as both the centrifugal BOB correction and the Ω-doubling splittings have substantial effects on the predicted transition energies.

4. Results

Our challenge now is to determine the optimum form and polynomial order for the functions used to represent the exponent coefficients of the two MLR potentials, and for the A-state centrifugal BOB and Ω-doubling radial strength functions. Because fits in which one state or the other was represented by term values were relatively time consuming, we began with a cyclic approach of, in turn, optimizing the fit with regard to the parameters defining one of these states while holding the model for the other fixed, and then repeating the procedure for the other. However, in the end, all parameters for both states were fitted simultaneously.

The long-range tails $u_{\rm LR}(r)$ of all of the models used for both electronic states were three-term versions of the damped inverse-power sums of Eqs. (15) and (16) in which $m_i = 5$, 6 and 8, and except where stated otherwise, the inverse-power coefficients C_5, C_6, and C_8 were held fixed at the theoretical values of Saute et al. [45]. In view of the discussion of Section 3.3, this means that the integer p defining the dimensionless radial variables $y_p(r;\, r_e)$ and $y_p(r;\, r_{\rm ref})$ must be set to be $p > (m_{\rm last} - m_1) = (8-5) = 3$. Further, since the leading contribution associated with the long-range behaviour of the exponential term in the MLR form of Eq. (9) is a term with the inverse power $m_i = m_1 + p$, and the power associated with the third dispersion energy term in the theoretically predicted long-range potential is $m_4 = 10$ [47], this exponent-variable power was fixed at $p = 5$ for all of the cases considered below.

In general, the quality of fit improves with increases in the order N_β of the polynomial defining the potential function exponent coefficient $\beta(r)$ of Eq. (13). However, it tends to converge at different rates for different values of the radial-variable expansion centre $r_{\rm ref}$, and for different values of the power q defining the second dimensionless radial expansion variable, $y_q(r;\, r_{\rm ref})$. All else being equal, for larger values of q, larger values of N_β tend to be required to achieve a given quality of fit. However, for small values of q, the extrapolation properties of the potential are sometimes poor (see below). Performing fits to a variety of different models for the X state of Br_2 yielded the results shown in Fig. 5, and analogous results for the A state are shown in Fig. 6. In both, the predicted improvement in the quality-of-fit parameter $\overline{dd}$ with increasing N_β for given values of q and $r_{\rm ref}$ is easily seen, and as expected, the range of $r_{\rm ref}$ values that yields a "good" fit (i.e., minimum values

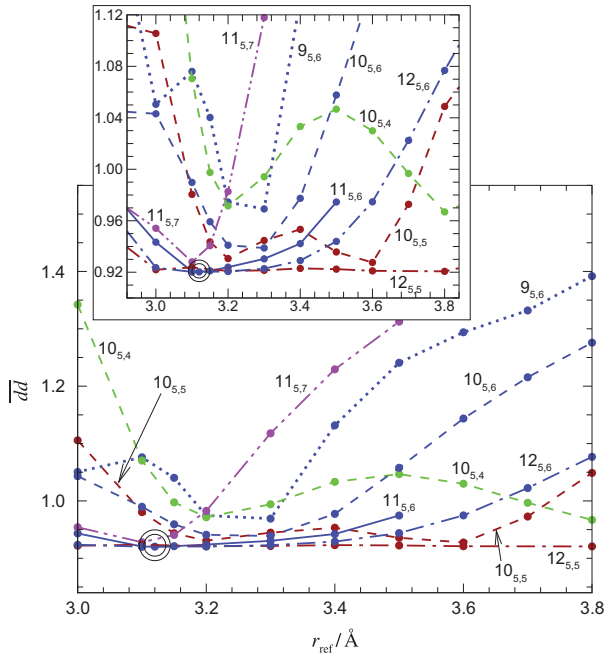

Fig. 5. Variation of the quality of fit $\overline{dd}$ with the radial variable expansion centre r_{ref} for a number of different MLR models for the $X^1\Sigma_g^+$ state of Br_2. The labels for the various cases are $N_{p,q}$, where $N \equiv N_\beta$.

of $\overline{dd}$) increases with N_β. However, there are clearly still a number of different {q, r_{ref}, N_β} combinations that will give a 'good' fit for either state.

An important test of the validity of a given fitted potential is whether it behaves well in the extrapolation region between the outer turning point of the highest observed level and the asymptotic limit where $r \to \infty$. This is a particularly relevant question for the $X^1\Sigma_g^+$ state, since the highest observed vibrational level ($v'' = 76$) is bound by 129 cm^{-1} and has an outer turning point of only 4.63 Å. While our long-range potential for the this state consists of three inverse-power terms with $m_i = 5$, 6 and 8, the C_5 coefficient is very small (and repulsive), and so the long-range tail $u_{LR}(r)$ consists mainly of inverse-power terms corresponding to $m_i = 6$ and 8. As a result, in the extrapolation region, a plot of $C_6^{eff}(r) \equiv r^6[\mathfrak{D} - V(r)]$ *vs.* $1/r^2$ should approach an $r \to \infty$ intercept of C_6^{theory} with a limiting slope of C_8^{theory}. Fig. 7 shows plots of this type associated with the optimum r_{ref} values for a number of the families (cases with the same N_β and q) of models considered in Fig. 5. It is immediately clear that outside the data region, all of the potential function models for which $q = 4$ or 5 behave unphysically by showing implausible extrema, while those with $q = 6$ and 7 smoothly approach the limiting slope from above, which is the behaviour one would wish for, since the first theoretically-predicted long-range term omitted from our $u_{LR}(r)$ model for the long-range potential is the attractive C_{10}/r^{10} term. While the $11_{5,7}^{3.10}$ model is also very good in this regard, its *lack* of positive limiting curvature away from the C_8 slope leads us to prefer the best $q = 6$ model. The fact that all of the curves for the fitted potentials in Fig. 7 dip below the dotted line for the nominal limiting slope at the $1/r^2 \to 0$ intercept merely reflects the presence of the very weak C_5 term in the long-range tails of those potentials. On the basis of the results summarized in Figs. 5 and 7 we therefore conclude that our recommended model for the $X^1\Sigma_g^+$ state of Br_2 is an MLR potential with $p = 5$, $q = 6$, $r_{ref} = 3.12$ Å, and $N_\beta = 11$. The values of the parameters defining this potential are listed in Table 2.

For the $A^3\Pi_{1u}$ state of Br_2, the highest observed vibrational level is bound by less than 2 cm^{-1} and has an outer turning point of approximately 9.2 Å. On an inverse-r scale this is relatively close to the limit $r \to \infty$. Since the leading long-range terms for this state correspond to $m_i = 5$ and 6, and the C_5 coefficient is *not* very small (as it is for the $X^1\Sigma_g^+$ state), this means that the appropriate long-range extrapolation test would be a plot of $C_5^{eff} \equiv r^5[\mathfrak{D} - V(r)]$ *vs.* $1/r$, which should have an $1/r \to 0$ intercept of C_5^{theory} and a limiting slope of C_6^{theory}. Fig. 8 shows plots of this type for models associated with the optimum-r_{ref} values for a number of the cases considered in Fig. 6. It is immediately clear that *all* of these models behave sensibly in the long-range extrapolation region. We are therefore free to choose our recommended potential function model for the $A^3\Pi_{1u}$ state so as to satisfy the objectives of minimizing the number of empirical potential function expansion parameters (i.e., minimizing N_β), and optimizing the quality of fit (i.e., minimizing $\overline{dd}$). This leads us to recommend an MLR potential with $p = 5$, $q = 4$ and $N_\beta = 13$ for representing the $A^3\Pi_{1u}$ state of Br_2.

Our remaining challenge is to determine optimum models for representing the centrifugal BOB correction function $\widetilde{R}_{na}^{Br}(r)$ and the Ω-doubling radial strength function $f_{\Omega 2}(r)$ for the $A^3\Pi_{1u}$ state

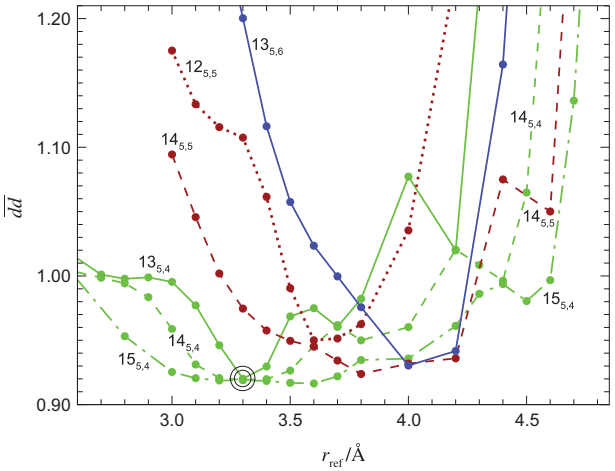

Fig. 6. Variation of the quality of fit $\overline{dd}$ with the radial variable expansion centre r_{ref} for a number of different MLR models for the $A^3\Pi_{1u}$ state of Br_2. The labels for the various cases are $N_{p,q}$, where $N \equiv N_\beta$.

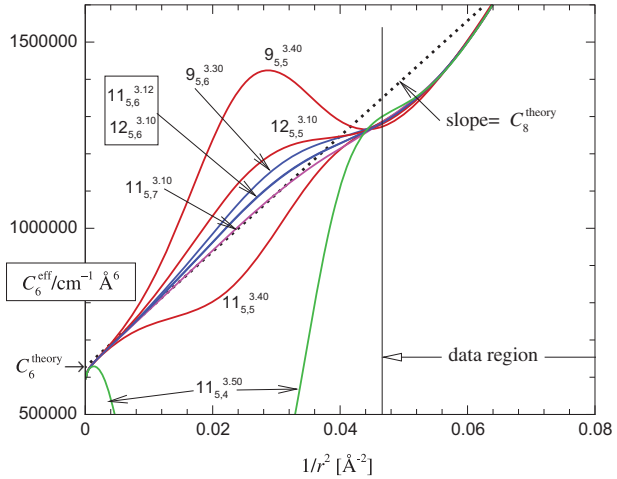

Fig. 7. Test of the long-range extrapolation behaviour of a number of fitted MLR models for the $X^1\Sigma_g^+$ state of Br_2 The labels for the various cases are $N_{p,q}^{r_{ref}}$, where $N \equiv N_\beta$.

Table 2
Parameters of the recommended models $MLR^{r_{ref}}_{p,q}(N_\beta)$ for the $A^3\Pi_{1u}$ and $X^1\Sigma^+_g$ states of Br_2, with energies in cm^{-1} and lengths in Å. Note that all β_i, t_i^{Br} and w_i^Ω are dimensionless. Numbers in parentheses are 95% confidence limit uncertainties in the last digits shown. Uncertainties are omitted for parameters lacking direct physical significance. This description uses $^{79,79}Br_2$ as the reference isotopologue, and the '*e*' levels as the reference energies for the Ω-doubling in the *A* state.

Form	$A^3\Pi_{1u}$ state $MLR^{3.30}_{5,4}(13)$	$X^1\Sigma^+_g$ state $MLR^{3.12}_{5,6}(11)$
T_e	13909.011 (12)	0.0
D_e	2147.864 (9)	16056.875 (2)
r_e	2.70432 (3)	2.2810272 (7)
ρ_{AB}	0.912	0.912
C_5	3.2×10^4	-3.3×10^2
C_6	6.37×10^5	6.274×10^5
C_8	1.55×10^7	1.55×10^7
{*p*, *q*}	{5, 4}	{5, 6}
r_{ref}	3.30	3.12
β_0	1.1554706	1.04182773
β_1	0.596137	0.861027
β_2	−3.17462	1.243753
β_3	−3.53635	0.166
β_4	10.62466	−1.48547
β_5	14.4571	−1.9263
β_6	−43.384	0.5519
β_7	−48.091	3.808
β_8	150.574	2.973
β_9	68.57	−1.523
β_{10}	−329.7	−3.380
β_{11}	52.9	−1.430
β_{12}	306.4	–
β_{13}	−181.0	–
$\{p_{ad}, q_{ad}\}$	{5, 5}	{6, 6}
u_0^{Br}	0.050 (46)	0.371 (42)
$\{p_{na}, q_{na}\}$	{3, 3}	–
t_0^{Br}	0.0	–
t_1^{Br}	0.00113	–
t_2^{Br}	0.02945	–
t_3^{Br}	−0.1809	–
t_4^{Br}	−0.571	–
t_5^{Br}	8.22	–
t_6^{Br}	−29.34	–
t_7^{Br}	49.9	–
t_8^{Br}	−41.9	–
t_9^{Br}	14.	–
w_0^Ω	0.00391	–
w_1^Ω	−0.0126	–
w_2^Ω	0.035	–
w_3^Ω	0.318	–

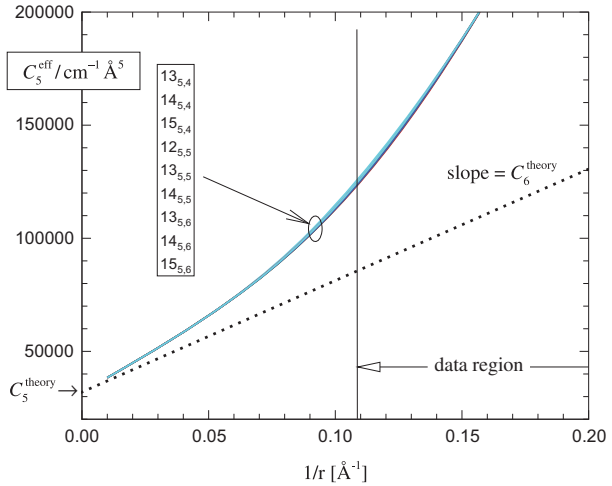

Fig. 8. Test of the long-range extrapolation behaviour of a number of fitted MLR models for the $A^3\Pi_{1u}$ state of Br_2 The labels for the various cases are $N^{r_{ref}}_{p,q}$, where $N \equiv N_\beta$.

of Br_2. These two properties are treated together because both make $J(J+1)$-dependent contributions to the level energies (see Eq. (5)), and hence might be expected to be highly correlated. Fig. 9 shows how the quality of fit varies with the number $(N_\Omega + 1)$ of terms used to represent $f_{\Omega}(r)$ in Eq. (20) when various choices are made for the order of polynomial N_{na} used to represent the centrifugal BOB radial function $\widetilde{R}^A_{na}(r)$ of Eq. (18). It is immediately clear that convergence with respect to the order of the Ω-doubling polynomial occurs at $N_\Omega = 3$, independent of the value of N_{na}. Moreover, Fig. 10 shows that the resulting Ω-doubling radial strength function is well-behaved and model-independent. Note that the conventional "band constant" parameters used to describe Ω-doubling as a function of v, commonly represented as q_v, may be generated as the radial expectation values of $\Delta V_\Omega(r)$ for different vibrational levels.

Unfortunately, Figs. 9 and 11 show that convergence with respect to the order of the centrifugal BOB strength function polynomial order is not as rapid as was the case for the Ω-doubling radial strength function. Moreover, Fig. 12 shows that the centrifugal BOB radial strength function determined in this way is not so well-defined and model-independent as was the case for the Ω-doubling radial strength function seen in Fig. 10. Nonetheless, all of the functions shown in Fig. 12 have the same basic shape: a minimum near r_e, a broad maximum around 4–7 Å and gradual fall-off at larger distances, and those for $N_{na} = 9$ and 10 are indistinguishable. Moreover, since it is the radial expectation value of this (very weak) function, weighted by the square of the vibrational wavefunction, that affects the actual level energies, the small oscillations and model-dependence seen in Fig. 12 are not too troubling. In any case, we select the $N_{na} = 9$ function as our recommended model for the centrifugal BOB radial strength function.

The parameters defining our final recommended models for the $X^1\Sigma^+_g$ and $A^3\Pi_{1u}$ states of Br_2 are summarized in Table 2. For the 16914 data for three isotopologues used in this study, these parameters yield a quality of fit corresponding to $\overline{dd} = 0.899$. The final fitted parameters shown in Table 2 were rounded off using the sequential rounding and refitting procedure of Ref. [54] that

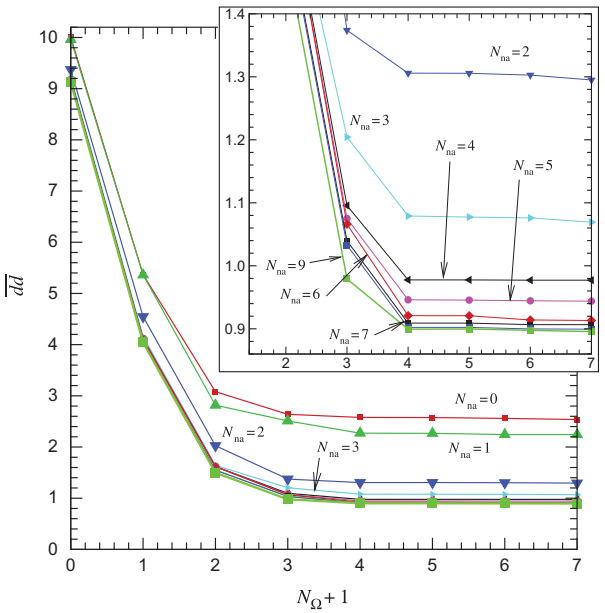

Fig. 9. Test of convergence of the fits as a function of N_Ω for different choices of the order N_{na} of the polynomial function used to represent the centrifugal BOB correction function.

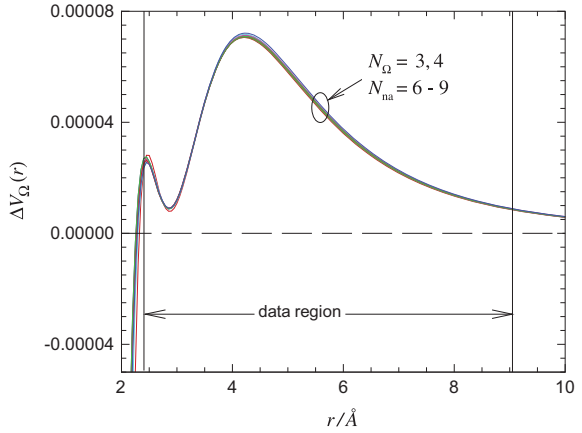

Fig. 10. $\Delta V_{\Omega}(r)$ functions yielded by fits to eight different models for the centrifugal BOB and Ω-doubling radial strength functions.

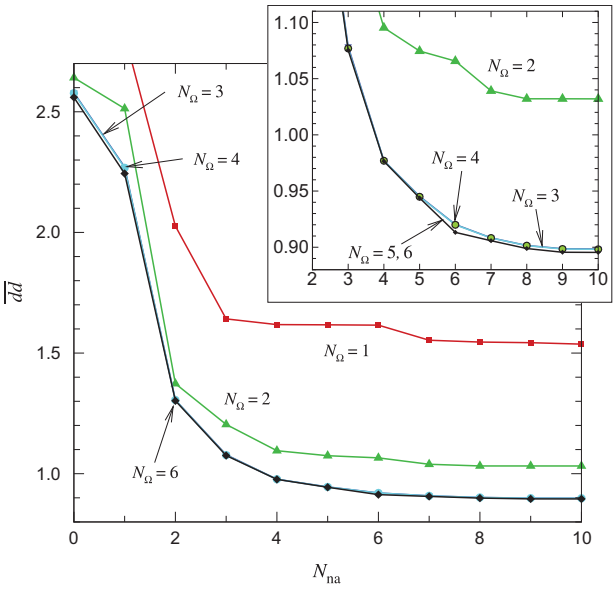

Fig. 11. Test of convergence of the fits as a function of N_{na} for different choices of the order N_Ω of the polynomial function used to represent the Ω-doubling radial strength function.

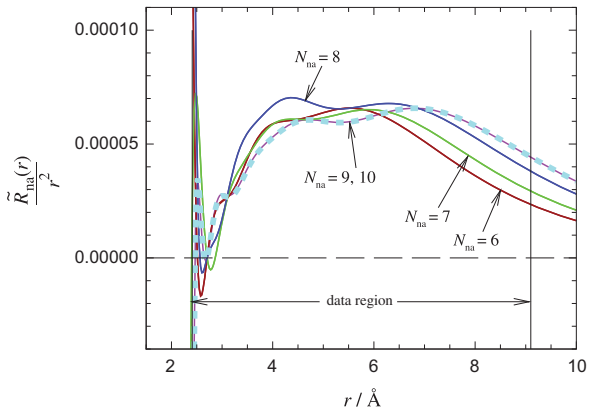

Fig. 12. Effective centrifugal BOB correction functions yielded by a optimized fits to a range of models.

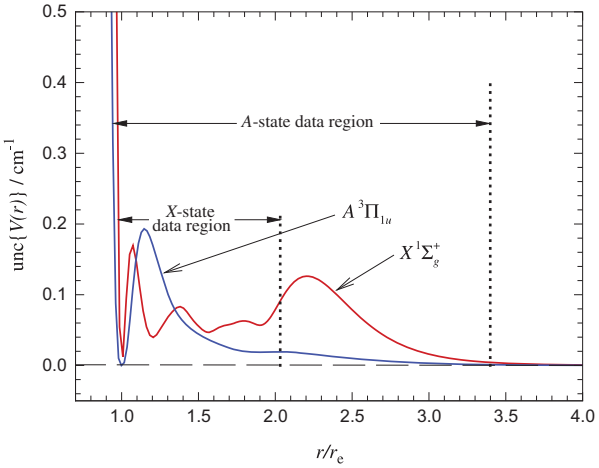

Fig. 13. Uncertainties in the final A- and X-state potential energy functions implied by the 95% confidence limit uncertainties in the potential function parameters yielded by the fit.

minimizes the number of significant digits required to represent the parameters determined by a fit without reducing the precision with which they represent the data. Uncertainties are not listed for parameters other than $\mathfrak{D}_e$ and r_e because, as is the case for higher-order Dunham coefficients in a conventional parameter-fit analysis, the individual parameters have no particular physical significance, so their uncertainties offers no insight. However, these parameters collectively provide a very accurate delineation of the two potential energy functions. Moreover, when those parameter uncertainties are combined with the correlation matrix from the fit, it is a straightforward matter to calculate the uncertainties in the resulting potential functions at any given distance (see Eq. (7) of Ref. [54]). Fig. 13 presents plot of the 95% confidence limit uncertainties in our recommended X and A-state potential energy functions generated in this way. A FORTRAN subroutine for generating the recommended potentials, together with lists of the band constants $\{G_v, B_v, D_v, \ldots\}$, and (for the $A^3\Pi_{1u}$ state) q_v, for all bound levels of all three isotopologues, have been submitted to the Journal's online Supplementary data archive.

As discussed at the end of Section 3, we believe that the present analysis can determine the isotopologue-dependence of the A–X electronic transition energy more reliably than it can the isotopologue-dependence of the individual potential energy well depths $\mathfrak{D}_e$ of the two states. To justify this conclusion, Table 3 presents results obtained from fits to our final model in which either none, or one, or both of the leading adiabatic BOB parameters $u_0(X)$ and $u_0(A)$ was allowed to vary. The values of the quality-of-fit parameter $\overline{dd}$ clearly indicate that at least one of these parameters can be determined from the data, and there is a small (1%) preference for that being the u_0^{Br} value for the $X^1\Sigma_g^+$ state. We choose the case in

Table 3
Test of the BOB dependence of the well-depth and electronic transition energy isotopomer shifts: $\delta(P) \equiv P(^{81,81}Br_2)$–$P(^{79,79}Br_2)$. $\delta\mathfrak{D}_e$, δT_e and $u_0(X/A)$ are all in cm^{-1}, while $\overline{dd}$ is dimensionless.

$u_0(X)$	$u_0(A)$	$\overline{dd}$	$\delta\mathfrak{D}_e\left(X^1\Sigma_g^+\right)$	$\delta\mathfrak{D}_e(A^3\Pi_{1u})$	$\delta T_e(A-X)$
0.0[a]	0.0[a].	1.10941	0.0	0.0	0.0
0.0[a]	−0.356 (8)	0.90615	0.0	0.018	−0.018
+0.326 (7)	0.0[a]	0.89874	−0.016	0.0	−0.016
+0.372 (42)	+0.052 (48)	0.89862	−0.018	−0.003	−0.016

[a] Value fixed at zero in the fit.

Table 4
Isotopologue-dependence of well depths and the electronic transition energy for the $A^3\Pi_{1u}$ and $X^1\Sigma_g^+$ states of Br_2, all in units of cm^{-1}. Numbers in parentheses are 95% confidence limit uncertainties in the last digits shown.

Isotopologue	$\mathfrak{D}_e\left(X^1\Sigma_g^+\right)$	$\mathfrak{D}_e(A^3\Pi_{1u})$	$T_e(A–X)$
$^{79,79}Br_2$	16056.875 (2)	2147.864 (9)	13909.011 (12)
$^{79,81}Br_2$	16056.866 (2)	2147.863 (9)	13909.003 (12)
$^{81,81}Br_2$	16056.857 (2)	2147.862 (9)	13908.995 (12)

which both u_0 values are allowed to vary as our recommended model because it provides more realistic estimates of the uncertainties. However, the fact that the electronic isotope shift is virtually the same for all of the last three cases considered in Table 3 gives us confidence regarding its physical significance. Note that it has the same sign and magnitude as the $B–X$ electronic isotope shift reported by Booth et al. ($-0.0129\ (20)\ cm^{-1}$) [55].

Table 4 lists the values of the well depths and electronic transition energy for the three isotopologues implied by the recommended parameter sets of Table 2. Note that to generate a potential for one of the 'minor isotopologues' ($^{79,81}Br_2$ or $^{81,81}Br_2$) one should not replace the $\mathfrak{D}_e$ value in Table 2 by the associated value from Table 4, but rather one should add the appropriate adiabatic correction function $\Delta V_{ad}^{(\alpha)}$ of Eq. (6) to the potential for the reference isotopologue $^{79,79}Br_2$. Since the radial strength function $\widetilde{S}_{ad}^{Br}$ for each state has only a single non-zero term (u_0^{Br}), this correction function is quite simple. For standard Franck–Condon factor and matrix element calculations, sample potential function input files for use in the standard program LEVEL can be found in the Journal's online Supplementary data archive.

5. Discussion

In many of the studies of the $B(^3\Pi_{0_u^+})$-state halogens, it became commonplace to use near-dissociation theory analyses [56–59] to obtain optimal estimates of the distance from the highest observed level to dissociation, of the number and energies of 'missing' levels, and of the leading long-range potential energy coefficient, C_5. However, the distance at which the C_5/r^5 term becomes the dominant contribution to the long-range potential is almost an order of magnitude larger for the $A^3\Pi_{1u}$ states [45,60], and so it is relatively much more difficult to determine values of their C_5 long-range coefficient from experimental data. Although most of the analyses reported herein were performed with all of the C_{m_i} coefficients held fixed at the values of Saute et al. [45], we also ran a couple of series of fits in which $C_5(A)$ was also treated as a free parameter. While the overall quality of fit improved slightly and the irregularity in the variation of $\overline{dd}$ with r_{ref} was somewhat reduced (c.f., Fig. 6), the model-dependence of the fitted C_5 values was sufficiently large that it was clear that no reliable empirical estimate of this C_5 coefficient may be obtained in this way.

The best previous estimate of the dissociation energy of Br_2 was that which Gerstenkorn and Luc obtained in 1989 [61] based on 16914 Fourier Transform data for the $B^3\Pi_{0^+u}$–$X^1\Sigma_g^+$ system of $^{79,79}Br_2$ extending to $v(B) = 53$, which is bound by only $5.3\ cm^{-1}$ [18]. They generated RKR turning points from Dunham G_v and B_v polynomials obtained from fits in which the first four centrifugal distortion constants were constrained to quantum-mechanical values calculated from the RKR potential in a self-consistent manner. A fit of their outermost RKR turning points to a simple (undamped) inverse-power sum then yielded values of $\mathfrak{D}$, C_5, C_6, C_8 and C_{10} for the B-state. On combining their $\mathfrak{D}$ value with the accurately-known atomic spin–orbit splitting energy [62] and their value for the ground-state zero-point energy [61], we obtain $\mathfrak{D}_e(X) = 16056.925\ (10)$ and $\mathfrak{D}_0(X) = 15894.545\ (10)\ cm^{-1}$. These values are $0.050\ cm^{-1}$ larger than those yielded by the present analysis: $\mathfrak{D}_e(X) = 16056.875\ (2)$ and $\mathfrak{D}_0(X) = 15894.495\ (2)\ cm^{-1}$. However, the fact that the binding energy of the highest observed level of the A state ($1.90\ cm^{-1}$) is more than a factor of two smaller than that for the B state gives us confidence in preferring the present results.

The lowest level of the $A^3\Pi_{1u}$ state used in the present analysis is the $v(A) = 2$ level observed in the present work [63]. However, a number of years ago Hwang et al. [15] reported the determination of $T_0(A)$ values with estimated relative uncertainties of $0.05\ cm^{-1}$ and an absolute uncertainty of $0.3\ cm^{-1}$ for the three isotopologues of Br_2 from a study of $\beta \leftarrow A$ transitions in a free jet expansion. The reason for our neglect of their $v(A) = 0$ observations was that we found them to be incompatible with any reasonable extrapolation from the present work. In particular when synthetic 0–0 band $X–A$ transitions for $^{79,79}Br_2$ generated from the parameters reported in Ref. [15] and the ground-state constants of Gerstenkorn et al. [18] were included in our analysis, they were found to be consistently $0.5\ cm^{-1}$ larger than predictions yielded by the fit. However,

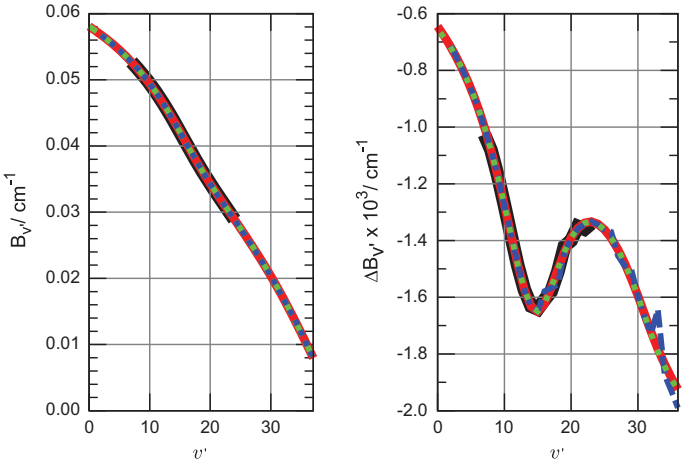

Fig. 14. Values of $B_{v'}$ (left-hand panel), and first differences $\Delta B_{v'} \equiv B_{v'+1} - B_{v'}$ (right-hand panel) between inertial rotational constants for the $A^3\Pi_{1u}$ state. The dotted blue curve shows results from the present fit to Eq. (1) and the solid black points come from the 1972 results of Coxon [8], while the (superimposed) solid red and broken green curves pass through values generated from potential-fit analyses that, respectively, did and did not allow for the centrifugal BOB correction. (For interpretation of the references to colour in this figure legend, the reader is referred to the web version of this article.)

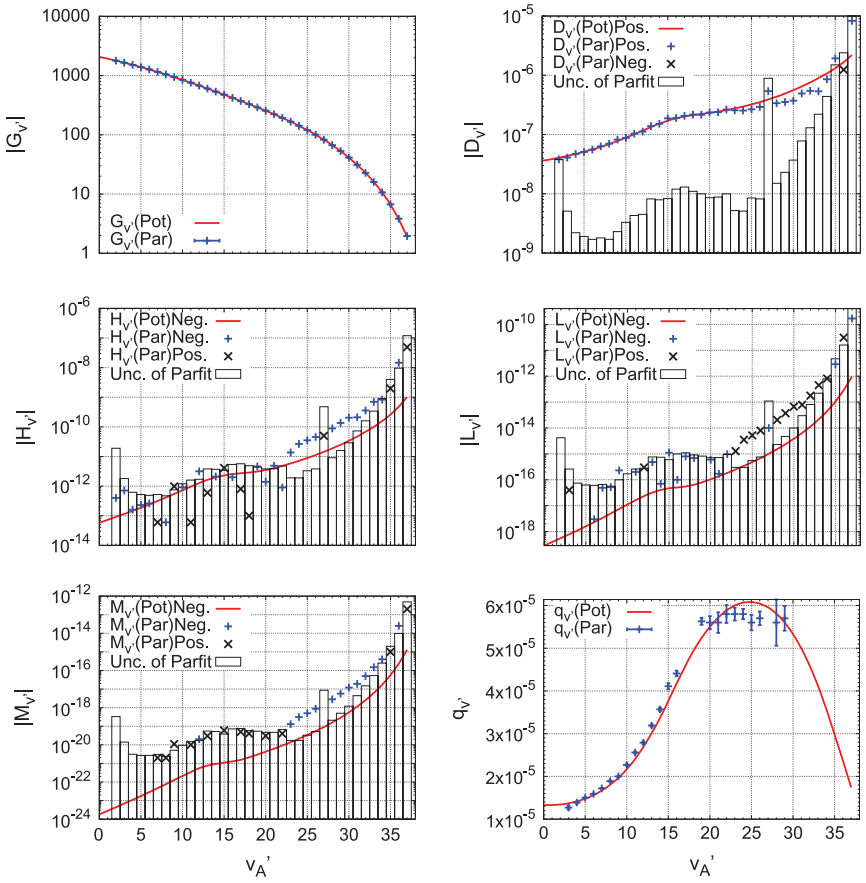

Fig. 15. Comparison of "parameter-fit" values of the band constants for the $A^3\Pi_{1u}$ state of $^{79,79}Br_2$, all in cm^{-1} (blue or black points, with error bars or boxes indicating uncertainties), with values generated from the recommended MLR potential (red curves). 'Neg.' and 'Pos.' mean that the values are negative and positive, respectively.

this difference is only slightly larger than the estimated absolute uncertainty of Ref. [15].

The original "parameter-fit" analysis of Boone [16] reported what appear to be an anomalous fluctuation in the v-dependence of the first differences $\Delta B_v \equiv B_{v+1} - B_v$ between the values of the leading rotational constants for the $A^3\Pi_{1u}$ state [16]. This behaviour is shown in the right-hand panel of Fig. 14, and the leading centrifugal distortion constants showed analogous behaviour. Since that behaviour was first discerned in a "parameter-fit" analysis, we were initially concerned that it might reflect non-mechanical perturbative effects. However, we found that it was fully accounted for by the analytic potential energy functions yielded by our DPF analysis, with the resulting potential curve(s) showing no anomalous behaviour in this region. We therefore conclude that this apparently anomalous behaviour of ΔB_v merely reflects some minor change in the shape of the A-state potential in this region. For the record, Fig. 15 compares values of the band constants for the $A^3\Pi_{1u}$ state obtained from a conventional "parameter fit" analysis using Eq. (1) with those generated from the present MLR potential. Note that the potential-fit values of the Ω-doubling parameter $q_{v'}$(Pot) shown here were calculated as expectation values of the function $\Delta V_{\Omega}^{\{\alpha\}}(r)$ of Eq. (8).

Finally, Fig. 16 shows the MLR potential curves for the $A^3\Pi_{1u}$ (solid black curves) and $X^1\Sigma_g^+$ (red curves) states yielded by our DPF analysis, together with an RKR potential for the $A'3\Pi_{2u}$ state computed by Sur and Tellinghuisen [64] and Van Marter et al. [65] (blue curves). It is clear that the outer walls of these three

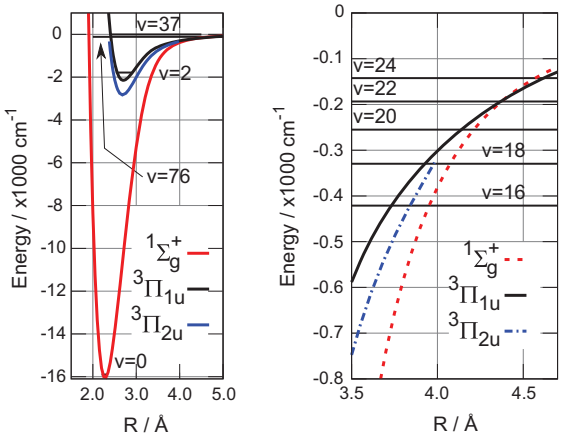

Fig. 16. The present MLR potentials for the $A^3\Pi_{1u}$ and $X^1\Sigma_g^+$ states of Br_2, together with the potential curve for the $A'^3\Pi_{2u}$-state reported by Sur and Tellinghuisen [64] and Van Marter et al. [65]. (For interpretation of the references to colour in this figure legend, the reader is referred to the web version of this article.)

potentials tend to merge at internuclear distances $\gtrsim 4$ Å and less than 300 cm^{-1} from the dissociation limit. The outer turning points of vibrational levels $v'(A) \gtrsim 20$ lie in this region. The $A^3\Pi_{1u}$ state of a halogen dimer is able to be perturbed by the $A'3\Pi_{2u}$ and the $B^3\Pi_{0_u^+}$ states through a type of spin–orbit interaction, as reported

by Ishiwata et al. in their analysis of the $A^3\Pi_{1u}$ state of Cl_2 [66]. The combination of this coupling with an accidental vibrational degeneracy may be the source of the strong perturbations that made the data for $a(A) = 27$ sufficiently irregular that they could not be used in our analysis.

Acknowledgments

We are very grateful to Mr. David Postell and Professor David Dolson for permitting us to use their unpublished *B*–*X* emission data in our analysis. C.B. and I.O. also very gratefully acknowledge enriching discussions with Professor F.W. Dalby. We also thank Professor Scott Hopkins for his patient assistance with Fig. 2. R.J.L., C.D.B. and I.O. are pleased to acknowledge financial support by the Natural Sciences and Engineering Research Council of Canada.

Appendix A. Supplementary material

Supplementary data associated with this article consist of: (i) a listing of all of the experimental data used in the analysis, (ii) lists of the first 8 band constants for all vibrational levels of all 3 isotopologues, calculated from the recommended potential energy functions for the A and X states, (iii) sample data files for performing calculations with these potentials using the publicly available bound-state/Franck-Condon program "LEVEL" (see http://leroy.uwaterloo.ca/programs/), and (iv) a stand-alone Fortran subroutine for generating these potential energy functions. This material may be found in the online version at http://dx.doi.org/10.1016/j.jms.2012.12.006.

References

[1] H. Kuhn, Z. Phys. 39 (1926) 77.
[2] G. Nakamura, Mem. Coll. Sci. Kyoto A 9 (1926) 315.
[3] W.G. Brown, Phys. Rev. 38 (1931) 1179.
[4] O. Darbyshire, Proc. Roy. Soc. (London) A 159 (1937) 93.
[5] J.A. Horsley, J. Mol. Spectrosc. 22 (1967) 469.
[6] M.A.A. Clyne, J.A. Coxon, J. Mol. Spectrosc. 23 (1967) 258.
[7] J.A. Coxon, M.A.A. Clyne, J. Phys. B 3 (1970) 1164.
[8] J.A. Coxon, J. Mol. Spectrosc. 41 (1972) 438.
[9] J.A. Coxon, J. Mol. Spectrosc. 41 (1972) 566.
[10] J.C.D. Brand, A.R. Hoy, S.M. Jaywant, A.W. Taylor, J. Mol. Spectrosc. 123 (1987) 84.
[11] T. Ishiwata, T. Hara, O. K, I. Tanaka, J. Chem. Phys. 87 (1987) 2513.
[12] T. Ishiwata, K. Obi, I. Tanaka, J. Mol. Spectrosc. 127 (1988) 353.
[13] I. T, K. Obi, I. Tanaka, J. Chem. Phys. 91 (1989) 3306.
[14] T. Ishiwata, T. Hara, K. Obi, I. Tanaka, J. Phys. Chem. 95 (1991) 2763.
[15] E. Hwang, P.J. Dagdigian, J. Tellinghuisen, J. Mol. Spectrosc. 181 (1997) 297.
[16] C.D. Boone, PhD Thesis, University of British Columbia, 1999. Note that parameter s_3 in Table 5-5 should be negative.
[17] C.D. Boone, F.W. Dalby, I. Ozier, J. Chem. Phys. 113 (2000) 8594.
[18] S. Gerstenkorn, P. Luc, A. Raynal, J. Sinzelle, J. Phys. 48 (1987) 1685.
[19] C. Focsa, H. Li, P.F. Bernath, J. Mol. Spectrosc. 200 (2000) 104.
[20] D. Postell, M.Sc thesis, Department of Chemisty, Wright State University, Fairborn, Ohio, 2005.
[21] D. Postell, D. Dolson, G. Perram, Unpublished Work, 2012.
[22] P. Venkateswarlu, V.N. Sarma, Y.V. Rao, J. Mol. Spectrosc. 96 (1982) 247.
[23] H.M. Pickett, Appl. Opt. 19 (1980) 2745.
[24] T. Yukiya, N. Nishimiya, M. Suzuki, J. Mol. Spectrosc. 269 (2011) 193.
[25] J.M. Brown, J. Mol. Spectrosc. 56 (1975) 159.
[26] N. Nishimiya, Y. Yukiya, M. Suzuki, J. Mol. Spectrosc. 163 (1994) 43.
[27] T. Yukiya, N. Nishimiya, M. Suzuki, J. Mol. Spectrosc. 182 (1997) 271.
[28] T. Yukiya, N. Nishimiya, M. Suzuki, J. Mol. Spectrosc. 214 (2002) 132.
[29] R.J. Le Roy, J. Seto, Y. Huang, DPotFit 1.2: A Computer Program for fitting Diatomic Molecule Spectra to Potential Energy Functions, University of Waterloo Chemical Physics Research Report CP-664 (2007). <http://www.leroy.uwaterloo.ca/programs/>.
[30] Y. Huang, R.J. Le Roy, J. Chem. Phys. 119 (2003) 7398;
Y. Huang, R.J. Le Roy, J. Chem. Phys. 126 (2007) 169904.
[31] R.J. Le Roy, R.B. Bernstein, J. Chem. Phys. 54 (1971) 5114.
[32] R.J. Le Roy, W.-K. Liu, J. Chem. Phys. 69 (1978) 3622.
[33] J.K.G. Watson, J. Mol. Spectrosc. 80 (1980) 411.
[34] J.K.G. Watson, J. Mol. Spectrosc. 223 (2004) 39.
[35] R.J. Le Roy, J. Mol. Spectrosc. 194 (1999) 189.
[36] R.J. Le Roy, D.R.T. Appadoo, K. Anderson, A. Shayesteh, I.E. Gordon, P.F. Bernath, J. Chem. Phys. 123 (2005) 204304.
[37] R.J. Le Roy, Determining equilibrium structures and potential energy functions for diatomic molecules, in: J. Demaison, A.G. Csaszar (Eds.), Equilibrium Structures of Molecules, Taylor & Francis, London, 2011, pp. 159–203 (Chapter 6).
[38] R.J. Le Roy, C.C. Haugen, J. Tao, H. Li, Mol. Phys. 109 (2011) 435.
[39] H. Margenau, Rev. Mod. Phys. 11 (1939) 1.
[40] J.O. Hirschfelder, C.F. Curtiss, R.B. Bird, Molecular Theory of Gases and Liquids, Wiley, New York, 1964.
[41] J.O. Hirschfelder, W.J. Meath, in: J.O. Hirschfelder (Ed.), Intermolecular Forces, Adv. Chem. Phys., vol. 12, Interscience, New York, 1967, pp. 3–106 (Chapter 1).
[42] T.Y. Chang, Rev. Mod. Phys. 39 (1967) 911.
[43] H. Kreek, W.J. Meath, J. Chem. Phys. 50 (1969) 2289.
[44] G.C. Maitland, M. Rigby, E.B. Smith, W.A. Wakeham, Intermolecular Forces-Their Origin and Determination, Oxford University Press, Oxford, UK, 1981.
[45] M. Saute, M. Bussery, M. Aubert-Frécon, Mol. Phys. 51 (1984) 1459.
[46] C. Douketis, G. Scoles, S. Marchetti, M. Zen, A.J. Thakkar, J. Chem. Phys. 76 (1982) 3057.
[47] R.J. Le Roy, R.D.E. Henderson, Mol. Phys. 105 (2007) 663.
[48] R.J. Le Roy, Y. Huang, J. Mol. Struct. (Theochem.) 591 (2002) 175.
[49] R.J. Le Roy, Y. Huang, C. Jary, J. Chem. Phys. 125 (2006) 164310.
[50] R.J. Le Roy, DParFit 3.3: A Computer Program for Fitting Multi-Isotopologue Diatomic Molecule Spectra, University of Waterloo Chemical Physics Research Report CP-660, 2005. <http://www.leroy.uwaterloo.ca/programs/>.
[51] R. Rydberg, Z. Phys. 73 (1931) 376;
O. Klein, Z. Phys. 76 (1932) 226;
R. Rydberg, Z. Phys. 80 (1933) 514;
A.L.G. Rees, Proc. Phys. Soc. 59 (1947) 998.
[52] R.J. Le Roy, `RKR1 2.0`: A Computer Program Implementing the First-Order RKR Method for Determining Diatomic Molecule Potential Energy Curves, University of Waterloo Chemical Physics Research Report CP-657 (2003); see http://www.leroy.uwaterloo.ca/programs/.
[53] R.J. Le Roy, `betaFIT 2.0`: A Computer Program to Fit Potential Function Points to Selected Analytic Functions, University of Waterloo Chemical Physics Research Report CP-665 (2009); see http://www.leroy.uwaterloo.ca/programs/.
[54] R.J. Le Roy, J. Mol. Spectrosc. 191 (1998) 223.
[55] J.L. Booth, I. Ozier, F.W. Dalby, J. Mol. Spectrosc. 210 (2001) 146.
[56] R.J. Le Roy, R.B. Bernstein, Chem. Phys. Lett. 5 (1970) 42–44;
R.J. Le Roy, R.B. Bernstein, J. Chem. Phys. 52 (1970) 3869–3879.
[57] R.J. Le Roy, in Molecular Spectroscopy, edited by R.N. Barrow, D.A. Long, and D.J. Millen (Chemical Society of London, London, 1973), Vol. 1, Specialist Periodical Report 3, pp. 113–176.
[58] R.J. Le Roy, W.-H. Lam, Chem. Phys. Lett. 71 (1980) 544.
[59] R.J. Le Roy, J. Chem. Phys. 101 (1994) 10217.
[60] M. Saute, M. Aubert-Frécon, J. Chem. Phys. 77 (1982) 5639.
[61] S. Gerstenkorn, P. Luc, J. Phys. France 50 (1989) 1417.
[62] E. Luc-Koenig, C. Morillon, J. Vergès, Physica 70 (1973) 175.
[63] The 2.5 times longer extrapolation to the minimum explains why the uncertainty in the fitted A-state well depth is more than 4 times larger than that for the X state, for which the data extends to v(X) = 0 (see Tables 1 and 2).
[64] A. Sur, J. Tellinghuisen, J. Mol. Spectrosc. 88 (1981) 323.
[65] T.A. Van Marter, Y. Lu, M.C. Heaven, E. Hwang, P.J. Dagdigian, J. Tellinghuisen, J. Mol. Spectrosc. 177 (1996) 311.
[66] T. Ishiwata, A. Ishiguro, K. Obi, J. Mol. Spectrosc. 147 (1991) 300.